In-Plane Anomalous Hall Effect in $\mathcal{PT}$-Symmetric Antiferromagnetic Materials

Jin Cao,[1,2,*] Wei Jiang,[1,2,*] Xiao-Ping Li,[1,2] Daifeng Tu,[3,4] Jiadong Zhou,[1,2] Jianhui Zhou,[3,†] and Yugui Yao[1,2,‡]

[1]*Centre for Quantum Physics, Key Laboratory of Advanced Optoelectronic Quantum Architecture and Measurement (MOE), School of Physics, Beijing Institute of Technology, Beijing 100081, China*

[2]*Beijing Key Lab of Nanophotonics & Ultrafine Optoelectronic Systems, School of Physics, Beijing Institute of Technology, Beijing, 100081, China*

[3]*Anhui Key Laboratory of Condensed Matter Physics at Extreme Conditions, High Magnetic Field Laboratory, HFIPS, Anhui, Chinese Academy of Sciences, Hefei 230031, P. R. China*

[4]*Department of Physics, University of Science and Technology of China, Hefei 230026, P. R. China*

(Received 6 September 2022; revised 5 February 2023; accepted 21 March 2023; published 19 April 2023)

The anomalous Hall effect (AHE), a protocol of various low-power dissipation quantum phenomena and a fundamental precursor of intriguing topological phases of matter, is usually observed in ferromagnetic materials with an orthogonal configuration between the electric field, magnetization, and the Hall current. Here, based on the symmetry analysis, we find an unconventional AHE induced by the in-plane magnetic field (IPAHE) via the spin-canting effect in $\mathcal{PT}$-symmetric antiferromagnetic (AFM) systems, featuring a linear dependence of magnetic field and 2π angle periodicity with a comparable magnitude to conventional AHE. We demonstrate the key findings in the known AFM Dirac semimetal CuMnAs and a new kind of AFM heterodimensional VS_2-VS superlattice with a nodal-line Fermi surface and, also, briefly discuss the experimental detection. Our Letter provides an efficient pathway for searching and/or designing realistic materials for a novel IPAHE that could greatly facilitate their application in AFM spintronic devices. National Science Foundation

DOI: 10.1103/PhysRevLett.130.166702

Introduction.—The anomalous Hall effect (AHE) has played a vital role in understanding low-power dissipation quantum phenomena associated with the Berry phase [1–3] and the development of the field of topological phases of matter [4–8]. In analogy to the conventional Hall effect due to the Lorentz force [9], where the magnetic field, electric field, and Hall current are orthogonal to each other, the AHE was commonly considered in the same manner by replacing the magnetic field with static magnetization in ferromagnetic (FM) materials [10]. However, the essential ingredient for AHE, i.e., time-reversal ($\mathcal{T}$) symmetry breaking, does not enforce any constraint on the magnetization direction or related magnetisms [11,12]. In principle, it allows an unconventional AHE with the Hall current flows in the plane spanned by the magnetization or magnetic field and the electric field, that is, in-plane AHE (IPAHE). Because of its unique in-plane configuration, the IPAHE could potentially revolutionize promising spintronic applications similar to the unidirectional spin Hall magnetoresistance [13,14].

Several theoretical investigations based on the ideal two-dimensional (2D) electron gas and a few artificially designed 2D material systems have shown the possible quantized version of the IPAHE with broken both $\mathcal{T}$ and mirror ($\mathcal{M}$) symmetries [15–18], most of which focus on FM or ferrimagnetic materials with an intrinsic in-plane magnetization. Meanwhile, recent studies have reached a consensus on the Berry curvature contribution to the intrinsic AHE due to spin-orbit coupling (SOC) [18–20], leading to the discovery of the AHE in antiferromagnetic (AFM) systems with a zero net magnetization [19–28]. Those inspire us to study the IPAHE among the large family of AFM systems, such as the $\mathcal{PT}$-symmetric AFM materials, usually with only a nonzero high-order AHE but a vanishing first-order AHE [29–32]. In reality, both the essential criterion for realizing the IPAHE and generally applicable searching and designing strategies for promising IPAHE materials are still lacking.

In this Letter, we find a universal symmetry rule to achieve the IPAHE, i.e., the absence of both rotation and reflection symmetries in at least two directions for the corresponding magnetic point group (MPG). We further elaborate on our key findings in one collinear ($\mathcal{PT}$-symmetric) AFM model system with only one direction having mirror reflection symmetry, which shows a noticeable AHE induced by an in-plane magnetic field. The complete list of MPGs allowing the IPAHE is given. To facilitate material discovery, we provide two feasible approaches, i.e., the top-down and bottom-up approaches, to design realistic AFM materials that support the IPAHE. In addition, the experimental detection and verification of the IPAHE with two representative examples are discussed.

Symmetry analysis.—The intrinsic anomalous Hall conductivity (AHC) evaluated by the integration of the Berry

curvature over the Brillouin zone, is usually proportional to the magnetization [33,34]. By expanding AHC up to the linear order of magnetization, one can define a rank-two tensor

$$\chi_{\alpha\beta} = \frac{\partial \sigma_\alpha}{\partial M_\beta}, \tag{1}$$

where M_β denotes the magnetic moment per unit cell, and $\sigma_\alpha = \frac{1}{2}\epsilon_{\alpha\beta\gamma}\sigma_{\beta\gamma}$ is the Hall pseudovector with the Levi-Civita symbol $\epsilon_{\alpha\beta\gamma}$ defining the antisymmetric dissipationless part of the linear conductivity tensor $\sigma_{\beta\gamma}$. The tensor χ, by definition, is independent of M_β, and should respect the symmetry of the system at $M_\beta = 0$. The diagonal parts of χ give the normal out-of-plane AHC, e.g., χ_{zz} [35], whereas the off-diagonal parts, e.g., χ_{zy}, represent the IPAHE [36]. Therefore, the tensor χ provides a complete description of the intrinsic AHE in magnetic materials.

The normal AHE cannot be ruled out by any structural symmetry operations, while the IPAHE requires low symmetry of the system. Since the tensor χ is invariant under translation operations, and remains an even function under $\mathcal{T}$ and $\mathcal{P}$ symmetry operations, it is sufficient to consider the rotational or mirror part of a MPG operation [see more details in the Supplemental Material (SM) [38]]. For convenience, we introduced a short notation $\mathcal{S}_\gamma$, which represents a class of MPG operations including mirror $\mathcal{M}_\gamma = \mathcal{P}\mathcal{C}_{2\gamma}$, rotation $\mathcal{C}_{n\gamma}$, and their combination with $\mathcal{T}$ ($\mathcal{T}\mathcal{M}_\gamma$ and $\mathcal{T}\mathcal{C}_{n\gamma}$). Here, γ is the direction of the corresponding symmetry operations. Given that both σ_α and M_β are pseudovectors that transform in the same way under $\mathcal{S}_\gamma$, they should be simultaneously parallel or perpendicular to the direction of $\mathcal{S}_\gamma$ to avoid the elimination of $\chi_{\alpha\beta}$ by $\mathcal{S}_\gamma$. Since we focus on the IPAHE, i.e., $\alpha \neq \beta$, if there exists more than one direction of $\mathcal{S}_{\gamma_i}$, one cannot find a configuration that supports nonzero $\chi_{\alpha\beta}$, where the orthogonal σ_α and M_β are perpendicular to all of the γ_i directions. Therefore, we can obtain the essential (necessary and sufficient) symmetry rule for the nonzero IPAHE: the absence of $\mathcal{S}_\gamma$ in at least two directions for the corresponding MPG. The detailed constraint on the IPAHE tensor components under MPG operations are summarized in Table. I.

TABLE I. Constraint on the IPAHE tensor components $\chi_{\alpha\beta}$ ($\alpha \neq \beta$) under $\mathcal{S}_\gamma$ ($\gamma = x, y, z$) operations. The mark ✓ (✗) denotes symmetry allowed (forbidden) components.

	$\mathcal{S}_x$	$\mathcal{S}_y$	$\mathcal{S}_z$
χ_{xy}, χ_{yx}	✗	✗	✓
χ_{xz}, χ_{zx}	✗	✓	✗
χ_{yz}, χ_{zy}	✓	✗	✗

IPAHE in $\mathcal{PT}$-symmetric AFM system.—The IPAHE has been reported mostly in FM or ferrimagnetic systems with a nonzero net magnetization [15,18,50]. Here, we focus on the $\mathcal{PT}$-symmetric AFM system with vanishing magnetization to realize the IPAHE. Consider the simplest collinear AFM system, in the absence of an external magnetic field, as sketched in Fig. 1(c), there are two magnetic sublattices denoted as $\boldsymbol{m}_\tau$ ($\tau = A, B$), satisfying $\boldsymbol{m}_A = -\boldsymbol{m}_B$. Because of the $\mathcal{PT}$ symmetry, the Kramers degeneracy exists in the entire Brillouin zone, leading to the vanishing AHE. Considering that the Berry curvature is usually non-Abelian, one could obtain a finite AHE by removing the Kramers degeneracy [1].

By applying an external magnetic field $\boldsymbol{B}$ perpendicular to $\boldsymbol{m}_\tau$, the local magnetic moments will be slightly tilted accordingly due to the spin-canting effect, yielding $\boldsymbol{m}_\tau = \boldsymbol{m}_\tau^{(0)} + \boldsymbol{m}'_\tau$. The net magnetic moment per unit cell will be $\boldsymbol{M} = \boldsymbol{m}'_A + \boldsymbol{m}'_B$, which will lift the Kramers degeneracy, and bring in a finite Berry curvature [Fig. 1(d)]. Note that we mainly focus on the weak magnetic field region that does not need to consider spin-flop or spin-flip transition and the spin-canting effect can be understood as one small perturbation [51]. Therefore, the corresponding net magnetic moment is approximately linear in the magnetic field $\boldsymbol{M} \propto \boldsymbol{B}$. We note that the spin-canting induced magnetization and nonzero IPAHE in a $\mathcal{PT}$-symmetric AFM system is different from that in the ferrimagnetic systems with respect to the direction of net magnetization and

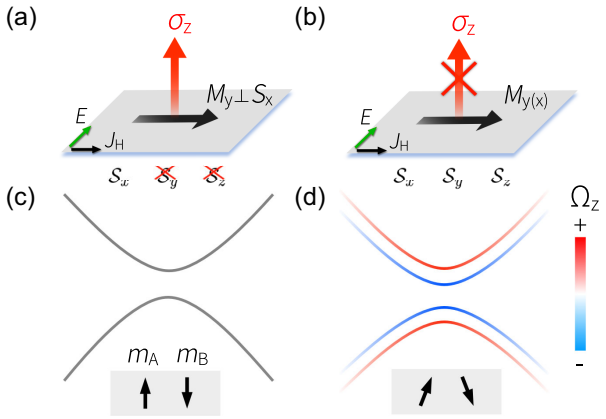

FIG. 1. Schematic rule for generating the IPAHE in $\mathcal{PT}$-symmetric AFM systems. (a) The IPAHE $\boldsymbol{J}_H = \boldsymbol{E} \times \boldsymbol{\sigma}$ is generated when the orthogonal σ_z and M_y are perpendicular to the direction of $\mathcal{S}_x$ (i.e., x direction). Here, $\mathcal{S}_x$ represents mirror $\mathcal{M}_x$, rotation $\mathcal{C}_{nx}$, and their combination with $\mathcal{T}$ ($\mathcal{T}\mathcal{M}_x$ and $\mathcal{T}\mathcal{C}_{nx}$). (b) Any two directions of $\mathcal{S}_\gamma(\gamma = x, y, z)$ together enforce a zero IPAHE. (c) The doubly degenerate band structure in the absence of an external magnetic field shows vanishing Berry curvature. The collinear AFM state is shown in black arrows. (d) The net magnetization is induced through the spin-canting effect. It lifts the band degeneracy, showing the opposite Berry curvature in the small-gap region, giving rise to the IPAHE.

dependence of magnetic field (see more discussion in SM [38]). Following the aforementioned symmetry analysis of the IPAHE, it is not forbidden to achieve the IPAHE in $\mathcal{PT}$-symmetric AFM systems, as also confirmed in the toy model [38].

Though the $\mathcal{PT}$-symmetric AFM systems widely exist in nature [52,53], the IPAHE in such systems has not yet been reported, probably due to limited material systems with required symmetries and less attention from both experimental and theoretical aspects. The predicted IPAHE in the $\mathcal{PT}$-symmetric AFM materials is one new kind of nonstandard Hall response and has a distinct microscopic nature and material realization from previous ones in either antiferromagnetic or low-symmetry systems [26,28,38,54]. To assist materials discovery, we provide a complete list of MPGs with $\mathcal{PT}$ symmetry that allow the IPAHE [38]. Further, to facilitate the experimental verification, we propose two general approaches to efficiently target suitable AFM materials that host the IPAHE, i.e., the top-down approach to engineer existing AFM materials and the bottom-up approach to design new materials.

Strained CuMnAs.—First, we demonstrate the IPAHE in well-established $\mathcal{PT}$-symmetric AFM systems. Since many of those materials may not meet the symmetry requirement for the IPAHE, it is necessary to apply feasible external field control to lower the structural symmetries. Hereafter, we term this searching method the top-down approach. With the advancement of modern technologies in fine tuning of material properties, various field control methods have been successfully applied in multiple material systems, such as electric field, strains, high pressure and chemical doping [55–57]. Here, we would examine the IPAHE in one well-known and typical $\mathcal{PT}$-symmetric AFM system, orthorhombic CuMnAs with Néel temperature $T_N \sim 300$ K [58–63], which notably exhibits significant potential in electrical switching of the AFM order [64] and terahertz electrical writing for memory [65].

The crystal structure of orthorhombic CuMnAs is shown in Fig. 2(a), where the AFM aligned magnetic moments are mainly concentrated on the Mn atoms along the b direction (AFM-b), as indicated by grey arrows, which has been observed in experiments [61]. The AFM-b state belongs to the MPG $m'mm$ [66,67], generated by $\mathcal{T}\mathcal{M}_x$, $\mathcal{M}_y$, and $\mathcal{M}_z$. It consists of $\mathcal{S}_\gamma$ operations in all three directions that prohibit the IPAHE. To lower the crystal symmetry, we applied a 2% shear strain in the a direction, as sketched in Fig. 2(b). The new AFM-b state has a lower symmetry $2'/m$, consisting of only $\mathcal{PT}$, $\mathcal{T}\mathcal{C}_{2y}$, and $\mathcal{M}_y$, i.e., only $\mathcal{S}_y$. The corresponding band structure under 2% shear strain is shown in Fig. 2(c), which preserves well the nodal-line structure on the $k_y = 0$ plane surrounding the X point near the Fermi level, as also confirmed by the Fermi surface plot in Fig. 2(d).

Because of the $\mathcal{S}_y$ symmetry, the nonzero IPAHE components are $\chi_{zx(xz)}$. The distributions of the calculated Berry curvature with spin-canting effect [38] are shown in Figs. 2(e) and 2(f). It is clear that the splitting of the doubly degenerate bands generates a nonzero Berry curvature near the gap opening area, leading to a finite IPAHE that will be discussed in detail later. We note that the magnetic ground state may change from AFM-b to AFM-c with a certain amount of hole doping [60]. Thus, we also tested the AFM-c state and confirmed that an IPAHE can also be achieved through proper strain engineering [38]. Note that the shear strain effect to the IPAHE is different from that to the conventional AHE, though the two show comparable variation in magnitude with the changing shear strain [38].

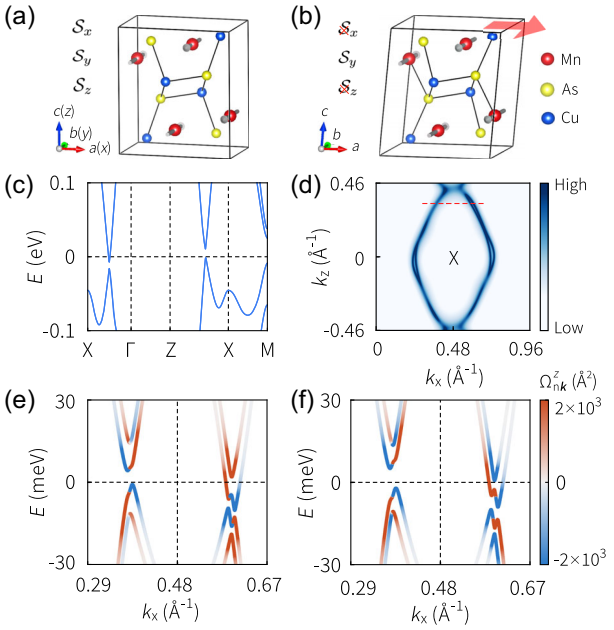

FIG. 2. The top-down approach to engineer IPAHE materials. (a) The AFM-b state of orthorhombic CuMnAs has $\mathcal{S}_\gamma$ in three directions that prohibits the IPAHE. (b) Schematic of the CuMnAs under shear strain along the a direction, which has only $\mathcal{S}_y$ symmetry, thus, allowing the IPAHE. (c) The band structure after shear strain. (d) The Fermi surface plot in the $k_y = 0$ plane at $E_F = 0$. (e) and (f) The Berry curvature distributions along the red dashed line in panel (d) with spin-canting effect $M_x = 0.4\ \mu_B$ and $M_z = 0.4\ \mu_B$ per unit cell, respectively.

Heterodimensional VS_2-VS *superlattice.*—Besides the top-down approach, one can take advantage of the recent rapid advancement of modern material synthesis through bottom-up design to create IPAHE materials, for example, in heterostructures [68,69]. Given the relatively low symmetry of one-dimensional (1D) materials, heterostructure systems formed by a combination of 1D and 2D or 3D materials could easily satisfy the aforementioned symmetry requirements. In fact, these heterostructures, i.e., heterodimensional, materials have been successfully synthesized in families of 3D transition metal chalcogenides, where 2D transition metal dichalcogenide (TMD) layers are connected through intercalated layers constructed by the same transition metal element with a typical 1D array pattern

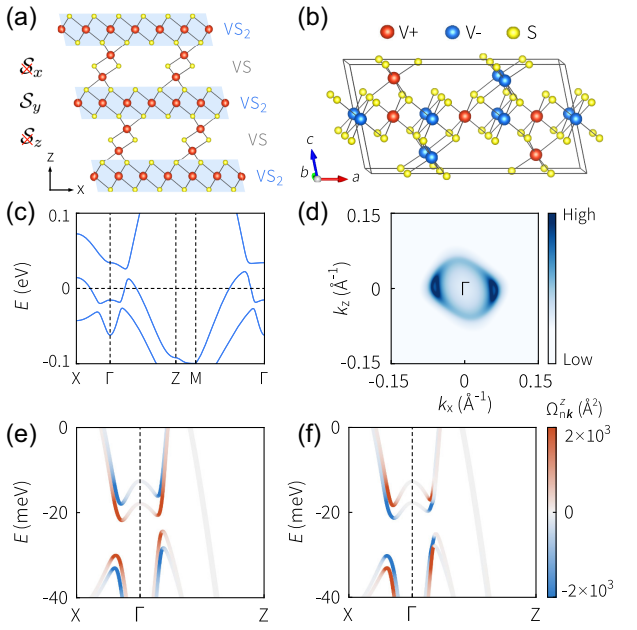

FIG. 3. The bottom-up approach to design IPAHE materials. (a) The heterodimensional superlattice consists of a 2D VS_2 and a 1D VS array that naturally meets the symmetry requirement of the IPAHE. (b) Sketch of the AFM-b state in the VS_2-VS superlattice. The notation V+ and V− denotes opposite local magnetic moments on the V atoms along b direction. (c) The band structure and (d) the density of states in the $k_y = 0$ plane at $E_F = -20$ meV. (e) and (f) The Berry curvature distributions with spin-canting effect $M_x = 0.4\ \mu_B$ and $M_z = 0.4\ \mu_B$ per unit cell, respectively.

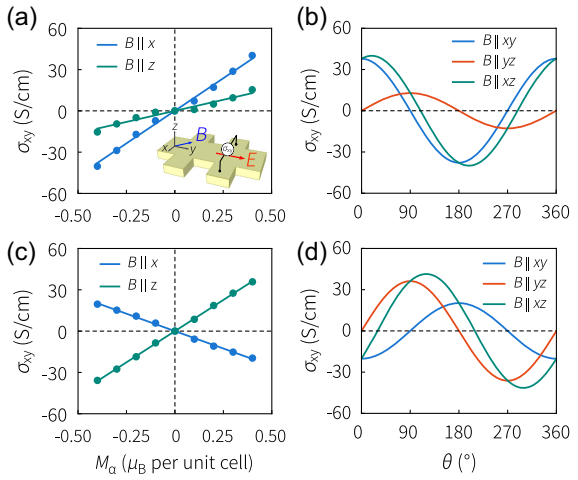

FIG. 4. The in-plane and normal AHC for strained CuMnAs in panels (a) and (b) and VS_2-VS superlattice in panels (c) and (d). In panels (a) and (c), the calculated results are shown as scatter diagrams, and the fitted results are given in solid lines. The panels (b) and (d) are the AHC under the arbitrary direction of the magnetic field. The Fermi levels were chosen near the nodal line. $E_F = -24$ meV and $E_F = -20$ meV were used for CuMnAs and VS_2-VS superlattice, respectively.

[68,69]. The intercalation of quasi-1D arrays could effectively reduce the symmetry of the heterodimensional system, which also provides one tunable pathway to modify the magnetization easy axis between the out-of-plane and in-plane directions. Here, we elaborate on the heterodimensional superlattice formed by a combination of 2D TMD and 1D transition-metal monochalcogenide array through the bottom-up approach, as shown in Fig. 3, and illustrate the corresponding IPAHE due to its designed structure with desired symmetry.

To reach the required symmetry, we follow the general stacking pattern of experiments with an alternating 2D TMD and 1D array layer by layer, as shown in Fig. 3(a). The nonmagnetic structure belongs to the C_{2h} point group with only one direction of mirror symmetry $\mathcal{M}_y$, which perfectly meets the symmetry requirement of the IPAHE. Furthermore, we selected the vanadium based materials and carried out first-principles calculations. We found the VS_2-VS superlattice prefers the AFM state with the magnetization aligned along the b direction with a calculated T_N about 14 K [38] as shown in Fig. 3(b), denoted as AFM-b. It belongs to MPG $2/m1'$ generated by $\mathcal{T}$, $\mathcal{P}$, and $\mathcal{M}_y$, i.e., only $\mathcal{S}_y$. Thus, we will use VS_2-VS as one representative example to demonstrate the intriguing IPAHE in heterodimensional materials.

In the absence of SOC, the band structure near the Fermi level is dominated by the nodal line on the $k_y = 0$ plane. At the Γ point, the two bands have opposite eigenvalues of $\mathcal{M}_y$, indicating this nodal line is protected by the $\mathcal{M}_y$ symmetry [70]. After including the SOC effect, there is a small gap near the nodal line, as shown in Figs. 3(c) and 3(d). Since the SOC effect respects the $\mathcal{PT}$, the energy bands remain doubly degenerate and the Berry curvature vanishes in the entire Brillouin zone, resulting in a vanishing AHE.

Because of the $\mathcal{S}_y$ symmetry, the nonzero IPAHE component is $\chi_{zx(xz)}$. Under the influence of the spin-canting effect due to the external magnetic field, the energy bands split and the Berry curvature becomes nonzero with a pronounced contribution near the gap opening area, as shown in Figs. 3(e) and 3(f). The resulting nonzero Berry curvature leads to a finite IPAHE similar to the strained CuMnAs. The band-resolved Berry curvature distribution shows that the Berry curvature hot spots are mainly distributed near the gap-opening region of the nodal line, which also exhibits the maximum IPAHE in the energy-resolved AHC [38].

Experimental signature.—We turn to the experimental detection of the IPAHE in a standard four-terminal Hall setup [inset of Fig. 4(a)]. In order to observe the IPAHE while suppressing the contribution from the orbital effect due to the Lorentz force [71], it is desirable to choose nanoflakes of the thickness in the range from several nm to tens of nm [38,72]. This can now be achieved experimentally through either mechanical exfoliation or chemical

vapor depositions. The strained CuMnAs and VS_2-VS superlattice have only the $\mathcal{S}_y$ symmetry, which imposes the same constraint on the IPAHE. The nonzero tensor elements are χ_{zx} and χ_{zz}. Then, the anomalous Hall conductivity can be given by

$$\sigma_{xy} = \chi_{zx} M_x + \chi_{zz} M_z. \tag{2}$$

The calculated AHC for CuMnAs and VS_2-VS are depicted in Figs. 4(a) and 4(c), respectively, showing a linear dependence relation in $\boldsymbol{M}$, similar to the conventional AHE in ferromagnets [34]. By fitting Eq. (2), we obtain $\chi_{zx} = 95\ \mathrm{S}/(\mathrm{cm}\cdot\mu_B)$ and $\chi_{zz} = 32\ \mathrm{S}/(\mathrm{cm}\cdot\mu_B)$ for strained CuMnAs, and $\chi_{zx} = -51\ \mathrm{S}/(\mathrm{cm}\cdot\mu_B)$ and $\chi_{zz} = 91\ \mathrm{S}/(\mathrm{cm}\cdot\mu_B)$ for VS_2-VS. Based on the fitted tensor χ, the AHC under any arbitrary direction of the magnetic field can be obtained from Eq. (2), as shown in Figs. 4(b) and 4(d) for CuMnAs and VS_2-VS, respectively. In general, there may exist higher order corrections of $\boldsymbol{M}$ in Eq. (2). Since the spin-canting induced magnetic moment per unit cell is very small ($M \ll 1\ \mu_B$), such corrections could be negligible.

It should be noted that considering the diversity of TMD materials and their combination with quasi-1D intercalated layers, such an IPAHE could widely exist in similar materials with the same structural symmetry, where the quantized version of the IPAHE could possibly be realized. We also point out that the extrinsic AHE originating from the side jump process usually shares the same scaling relation against the longitudinal conductivity as the intrinsic AHE [73].

Summary and discussion.—We have established a comprehensive rule of the IPAHE with minimum symmetry requirement and extend its material realization to a large family of $\mathcal{PT}$-symmetric AFM systems that have been rarely studied before [52,53,74]. In fact, the mechanism for an IPAHE can be straightforwardly applicable to other Berry phase related quantum phenomena, such as the anomalous Nernst effect and anomalous thermal Hall effect and, also, suitable for other compensated AFM systems beyond $\mathcal{PT}$-symmetric ones. Meanwhile, these $\mathcal{PT}$-symmetric AFM systems also provide a promising platform for exploring novel quantum phenomena and building energy-efficient AFM spintronic devices, which should draw immediate experimental attention.

We thank D.-F. Shao for helpful discussions. This work is supported by the National Key R&D Program of China (Grant No. 2020YFA0308800), the NSF of China (Grants No. 12234003, No. 12061131002, No. U2032164, No. 12174394, No. 62174013, and No. 92265111), the Strategic Priority Research Program of Chinese Academy of Sciences (Grant No. XDB30000000). W. J. was supported by the NSF of China (Grant No. 12204037) and the Beijing Institute of Technology Research Fund Program for Young Scholars. J. Z. was supported by the High Magnetic Field Laboratory of Anhui Province.

*These authors contributed equally to this work.
†jhzhou@hmfl.ac.cn
‡ygyao@bit.edu.cn

[1] D. Xiao, M.-C. Chang, and Q. Niu, Rev. Mod. Phys. **82**, 1959 (2010).
[2] J. Sinova, S. O. Valenzuela, J. Wunderlich, C. H. Back, and T. Jungwirth, Rev. Mod. Phys. **87**, 1213 (2015).
[3] V. Baltz, A. Manchon, M. Tsoi, T. Moriyama, T. Ono, and Y. Tserkovnyak, Rev. Mod. Phys. **90**, 015005 (2018).
[4] M. Z. Hasan and C. L. Kane, Rev. Mod. Phys. **82**, 3045 (2010).
[5] H. Weng, R. Yu, X. Hu, X. Dai, and Z. Fang, Adv. Phys. **64**, 227 (2015).
[6] A. Bansil, H. Lin, and T. Das, Rev. Mod. Phys. **88**, 021004 (2016).
[7] N. P. Armitage, E. J. Mele, and A. Vishwanath, Rev. Mod. Phys. **90**, 015001 (2018).
[8] B. Q. Lv, T. Qian, and H. Ding, Rev. Mod. Phys. **93**, 025002 (2021).
[9] E. H. Hall, Am. J. Math. **2**, 287 (1879).
[10] R. Karplus and J. M. Luttinger, Phys. Rev. **95**, 1154 (1954).
[11] N. Nagaosa, J. Sinova, S. Onoda, A. H. MacDonald, and N. P. Ong, Rev. Mod. Phys. **82**, 1539 (2010).
[12] C.-X. Liu, S.-C. Zhang, and X.-L. Qi, Annu. Rev. Condens. Matter Phys. **7**, 301 (2016).
[13] C. O. Avci, K. Garello, A. Ghosh, M. Gabureac, S. F. Alvarado, and P. Gambardella, Nat. Phys. **11**, 570 (2015).
[14] Y. Lv, J. Kally, D. Zhang, J. S. Lee, M. Jamali, N. Samarth, and J.-P. Wang, Nat. Commun. **9**, 111 (2018).
[15] X. Liu, H.-C. Hsu, and C.-X. Liu, Phys. Rev. Lett. **111**, 086802 (2013).
[16] P. Zhong, Y. Ren, Y. Han, L. Zhang, and Z. Qiao, Phys. Rev. B **96**, 241103(R) (2017).
[17] S. Sun, H. Weng, and X. Dai, Phys. Rev. B **106**, L241105 (2022).
[18] Z. Liu, G. Zhao, B. Liu, Z. F. Wang, J. Yang, and F. Liu, Phys. Rev. Lett. **121**, 246401 (2018).
[19] S. Nakatsuji, N. Kiyohara, and T. Higo, Nature (London) **527**, 212 (2015).
[20] A. K. Nayak, J. E. Fischer, Y. Sun, B. Yan, J. Karel, A. C. Komarek, C. Shekhar, N. Kumar, W. Schnelle, J. Kübler, C. Felser, and S. S. P. Parkin, Sci. Adv. **2**, e1501870 (2016).
[21] R. Shindou and N. Nagaosa, Phys. Rev. Lett. **87**, 116801 (2001).
[22] I. Martin and C. D. Batista, Phys. Rev. Lett. **101**, 156402 (2008).
[23] H. Chen, Q. Niu, and A. H. MacDonald, Phys. Rev. Lett. **112**, 017205 (2014).
[24] N. J. Ghimire, A. S. Botana, J. S. Jiang, J. Zhang, Y. S. Chen, and J. F. Mitchell, Nat. Commun. **9**, 3280 (2018).

[25] D.-F. Shao, S.-H. Zhang, G. Gurung, W. Yang, and E. Y. Tsymbal, Phys. Rev. Lett. **124**, 067203 (2020).

[26] L. Šmejkal, R. González-Hernández, T. Jungwirth, and J. Sinova, Sci. Adv. **6**, eaaz8809 (2020).

[27] J. Kipp, K. Samanta, F. R. Lux, M. Merte, D. Go, J.-P. Hanke, M. Redies, F. Freimuth, S. Blügel, M. Ležaić, and Y. Mokrousov, Commun. Phys. **4**, 99 (2021).

[28] Z. Feng, X. Zhou, L. Šmejkal, L. Wu, Z. Zhu, H. Guo, R. González-Hernández, X. Wang, H. Yan, P. Qin, X. Zhang, H. Wu, H. Chen, Z. Meng, L. Liu, Z. Xia, J. Sinova, T. Jungwirth, and Z. Liu, National electronics review **5**, 735 (2022).

[29] H. Liu, J. Zhao, Y.-X. Huang, W. Wu, X.-L. Sheng, C. Xiao, and S. A. Yang, Phys. Rev. Lett. **127**, 277202 (2021).

[30] C. Wang, Y. Gao, and D. Xiao, Phys. Rev. Lett. **127**, 277201 (2021).

[31] L. Šmejkal, A. H. MacDonald, J. Sinova, S. Nakatsuji, and T. Jungwirth, Nat. Rev. Mater. **7**, 482 (2022).

[32] S. Hayami, M. Yatsushiro, and H. Kusunose, Phys. Rev. B **106**, 024405 (2022).

[33] Y. Yao, L. Kleinman, A. H. MacDonald, J. Sinova, T. Jungwirth, D.-s. Wang, E. Wang, and Q. Niu, Phys. Rev. Lett. **92**, 037204 (2004).

[34] C. Zeng, Y. Yao, Q. Niu, and H. H. Weitering, Phys. Rev. Lett. **96**, 037204 (2006).

[35] L. D. Landau and E. M. Lifshitz, *Electrodynamics of Continuous Media* (Pergamon Press, New York, 1984).

[36] The IPAHE here comes from the antisymmetric part of off-diagonal components of the electric conductivity tensor. It should differ from the planar Hall effect that corresponds to the symmetric part of the off-diagonal components of electric conductivity and has the essential nature of anisotropic magnetoresistance [37].

[37] H. X. Tang, R. K. Kawakami, D. D. Awschalom, and M. L. Roukes, Phys. Rev. Lett. **90**, 107201 (2003).

[38] See Supplemental Material at http://link.aps.org/supplemental/10.1103/PhysRevLett.130.166702 for the symmetry requirements of the IPAHE, calculation details, an IPAHE of a four-band $\mathcal{PT}$-symmetric AFM model, more results of the IPAHE of CuMnAs, the calculated Néel temperature, and electronic susceptibility of the VS_2-VS superlattice, which include Refs. [39–49].

[39] A. P. Cracknell, Prog. Theor. Phys. **35**, 196 (1966).

[40] G. Kresse and J. Hafner, Phys. Rev. B **47**, 558 (1993).

[41] P. E. Blöchl, Phys. Rev. B **50**, 17953 (1994).

[42] J. P. Perdew, J. A. Chevary, S. H. Vosko, K. A. Jackson, M. R. Pederson, D. J. Singh, and C. Fiolhais, Phys. Rev. B **46**, 6671 (1992).

[43] J. P. Perdew, K. Burke, and M. Ernzerhof, Phys. Rev. Lett. **77**, 3865 (1996).

[44] S. Grimme, J. Antony, S. Ehrlich, and H. Krieg, J. Chem. Phys. **132**, 154104 (2010).

[45] S. L. Dudarev, G. A. Botton, S. Y. Savrasov, C. J. Humphreys, and A. P. Sutton, Phys. Rev. B **57**, 1505 (1998).

[46] A. A. Mostofi, J. R. Yates, G. Pizzi, Y.-S. Lee, I. Souza, D. Vanderbilt, and N. Marzari, Comput. Phys. Commun. **185**, 2309 (2014).

[47] G.-B. Liu, Z. Zhang, Z.-M. Yu, S. A. Yang, and Y. Yao, Phys. Rev. B **105**, 085117 (2022).

[48] Z. Zhang, G.-B. Liu, Z.-M. Yu, S. A. Yang, and Y. Yao, Phys. Rev. B **105**, 104426 (2022).

[49] J.-W. Rhim and Y. B. Kim, New J. Phys. **18**, 043010 (2016).

[50] H. Tan, Y. Liu, and B. Yan, Phys. Rev. B **103**, 214438 (2021).

[51] S. Blundell, *Magnetism in Condensed Matter* (Oxford University Press, New York, 2003).

[52] S. V. Gallego, J. M. Perez-Mato, L. Elcoro, E. S. Tasci, R. M. Hanson, K. Momma, M. I. Aroyo, and G. Madariaga, J. Appl. Crystallogr. **49**, 1750 (2016).

[53] S. V. Gallego, J. M. Perez-Mato, L. Elcoro, E. S. Tasci, R. M. Hanson, M. I. Aroyo, and G. Madariaga, J. Appl. Crystallogr. **49**, 1941 (2016).

[54] M. Seemann, D. Ködderitzsch, S. Wimmer, and H. Ebert, Phys. Rev. B **92**, 155138 (2015).

[55] W. Jiang, S. Zhang, Z. Wang, F. Liu, and T. Low, Nano Lett. **20**, 1959 (2020).

[56] W. Jiang, D. J. P. de Sousa, J.-P. Wang, and T. Low, Phys. Rev. Lett. **126**, 106601 (2021).

[57] D. Zhang, M. Bapna, W. Jiang, D. Sousa, Y.-C. Liao, Z. Zhao, Y. Lv, P. Sahu, D. Lyu, A. Naeemi, T. Low, S. A. Majetich, and J.-P. Wang, Nano Lett. **22**, 622 (2022).

[58] J. Mündelein and H.-U. Schuster, Z. Naturforsch. B **47**, 925 (1992).

[59] F. Máca, J. Mašek, O. Stelmakhovych, X. Martí, H. Reichlová, K. Uhlířová, P. Beran, P. Wadley, V. Novák, and T. Jungwirth, J. Magn. Magn. Mater. **324**, 1606 (2012).

[60] P. Tang, Q. Zhou, G. Xu, and S.-C. Zhang, Nat. Phys. **12**, 1100 (2016).

[61] E. Emmanouilidou, H. Cao, P. Tang, X. Gui, C. Hu, B. Shen, J. Wu, S.-C. Zhang, W. Xie, and N. Ni, Phys. Rev. B **96**, 224405 (2017).

[62] L. Šmejkal, J. Železný, J. Sinova, and T. Jungwirth, Phys. Rev. Lett. **118**, 106402 (2017).

[63] Vu Thi Ngoc Huyen, Y. Yanagi, and M.-T. Suzuki, Phys. Rev. B **104**, 035110 (2021).

[64] P. Wadley *et al.*, Science **351**, 587 (2016).

[65] K. Olejník, T. Seifert, Z. Kašpar, V. Novák, P. Wadley, R. P. Campion, M. Baumgartner, P. Gambardella, P. Němec, J. Wunderlich, J. Sinova, P. Kužel, M. Müller, T. Kampfrath, and T. Jungwirth, Sci. Adv. **4**, eaar3566 (2018).

[66] A. Bouhon, G. F. Lange, and R.-J. Slager, Phys. Rev. B **103**, 245127 (2021).

[67] C. J. Bradley and A. P. Cracknell, *The Mathematical Theory of Symmetry in Solids: Representation Theory for Point Groups and Space Groups* (Oxford University Press, New York, 2009).

[68] J. Zhou *et al.*, Nat. Mater. **22**, 450 (2022).

[69] J. Zhou *et al.*, Nature (London) **609**, 46 (2022).

[70] Note that there could be a charge density order in the VS_2-VS superlattice due to its unique heterodimensional structure and nodal-line structure [38].

[71] J. M. Ziman, *Electrons and Phonons. The Theory of Transport Phenomena in Solids* (Oxford University Press, New York, 1960).

[72] We note that the contribution to the Hall effect from Lorentz force and Berry curvature could be distinguished through temperature, thickness, and carrier density dependent measurements experimentally.

[73] L. Berger, Phys. Rev. B **2**, 4559 (1970).

[74] D.-F. Shao, G. Gurung, S.-H. Zhang, and E. Y. Tsymbal, Phys. Rev. Lett. **122**, 077203 (2019).